Accepted for BSSA on 30 January 2018

Source Modeling of an M_W 5.9 Earthquake in the Nankai Trough, Southwest Japan, using Offshore and Onshore Strong Motion Waveform Records

Kimiyuki Asano

Disaster Prevention Research Institute, Kyoto University, Gokasho, Uji, Kyoto 611-0011, Japan

Abstract

On 1 April 2016, an M_{W} 5.9 (M_{JMA} 6.5) plate-boundary earthquake occurred in the subduction zone of the Nankai Trough, offshore the Kii Peninsula, southwest Japan. This event is the largest plate-boundary earthquake in the source region after the 1944 Tonankai earthquake (M_{W} 8.0). In the last half century, moderate-to-large earthquakes of this focal type have become very rare in this region, and therefore, this event provides a good opportunity to investigate the source characteristics related to strong motion generation of subduction-zone plate-boundary earthquakes in the Nankai Trough. In this study, the source model of the earthquake was estimated on the basis of broadband strong motion waveform modeling using the empirical Green's function method. Source parameters of the strong motion generation area (SMGA) were optimized by waveform modeling in the frequency range 0.4–10 Hz. One SMGA is necessary to explain the observed waveforms at offshore and onshore strong motion stations. The best estimate of the size of the SMGA was 20.3 km^2, which does not follow the source scaling relationship for past plate-boundary earthquakes along the Japan Trench, northeast Japan. This result implies the possibility of differences between the source characteristics of plate-boundary events in the Nankai Trough and those along the Japan Trench. This

finding provides important information about regional variations of source characteristics in ground motion prediction for hazard assessment of future megathrust earthquakes.

Introduction

The Philippine Sea Plate subducts northwestward beneath southwest Japan along the Nankai Trough (e.g., Hashimoto and Jackson, 1993; Seno *et al.*, 1993), and the subduction of this oceanic plate has generated historical megathrust plate-boundary earthquakes (Ando, 1975). These earthquakes induced strong shaking and tsunamis across wide regions of the Japanese Islands. In order to estimate seismic hazards for such events, ground motion prediction on the basis of numerical simulations has been extensively studied for hypothetical megathrust earthquakes along the Nankai Trough (e.g., Miyake *et al.*, 2008; Sekiguchi *et al.*, 2008; Maeda *et al.*, 2016). Source heterogeneity is one of the key factors controlling the generation of strong ground motions (e.g., Miyake *et al.*, 2003). Thus, examining the regional characteristics of source parameters based on analysis of observed earthquakes is essential for improving ground motion prediction and seismic hazard assessment.

On 1 April 2016, an M_{JMA} 6.5 earthquake occurred offshore the Kii peninsula, southwest Japan at 11:39, Japan Standard Time (JST; 02:39, coordinated universal time [UTC]). This event was interpreted as a thrust-event on the plate boundary along the Nankai Trough (Wallace *et al.*, 2016). The centroid moment tensor (CMT) solution by the Global CMT Project (Ekström *et al.*, 2012) also supports that this event was a low-angle thrust earthquake. The hypocenter of this event is located inside the source fault of the 1944 Tonankai earthquake (M_W 8.0) (e.g., Ichinose *et al.*, 2003; Kikuchi *et al.*, 2003) (Figure 1) and other historical megathrust earthquakes (e.g., Ando, 1975). The last megathrust earthquake in this subduction zone was the 1944 Tonankai earthquake, after which the M_{JMA} 6.5 earthquake is the largest plate-boundary earthquake in the source region.

The significance of this event regarding seismic observations is that this event occurred beneath an ocean-bottom seismic network called the Dense Oceanfloor Network system for Earthquake and Tsunamis (DONET), which is jointly operated by the National Research Institute for Earth Science and Disaster Resilience (NIED) and Japan Agency for Marine-Earth Science and Technology (JAMSTEC) (Kaneda *et al.*, 2015). DONET1 consists of 20 ocean-floor stations, and each station has three-component strong motion accelerometers along with three-component broadband velocity sensors, pressure gauges, differential pressure gauges, hydrophone, and thermometer (Kaneda *et al.*, 2015).

The source characteristics of such events can be determined through broadband strong motion waveform modeling using the empirical Green's function method (Irikura, 1986; Miyake *et al.*, 2003). In this modeling, the source model is characterized by a strong motion generation area (SMGA) (Miyake *et al.*, 2003), which is defined as a rectangular area with high-stress drop or high slip-velocity. As the empirical Green's function method uses the observed record of a small event occurring close to the target event as a Green's function, the propagating-path and site effects are included in the empirical Green's function itself. Therefore, the SMGA source model based on the empirical Green's function method has high potential to reproduce ground motion time history in a broad frequency range. Strong motion modeling using the empirical Green's function method developed by Irikura (1986) has successfully reproduced observed strong ground motions for previous large subduction-zone plate-boundary earthquakes (e.g., Kamae and Kawabe, 2004; Suzuki and Iwata, 2007; Ramírez-Gaytán *et al.*, 2010; Takiguchi *et al.*, 2011; Asano and Iwata, 2012; Satoh, 2012; Kawabe and Kamae, 2013; Kurahashi and Irikura, 2013) as well as inland crustal (e.g., Kamae and Irikura, 1998; Miyake *et al.*, 2003; Suzuki and Iwata, 2006; Kurahashi *et al.*, 2008; Maeda *et al.*, 2008; Maeda and Sasatani, 2009; Yamamoto and Takenaka, 2009; Kurahashi and Irikura, 2010; Poiata *et al.*, 2012; Wen *et al.*, 2014; Riahi *et al.*, 2015; Xia *et al.*, 2015; Wen *et al.*, 2017) and intraslab earthquakes (e.g., Asano *et al.*, 2003; Morikawa and

Sasatani, 2004; Oth *et al.*, 2007; Poiata and Miyake, 2017).

The study of such earthquakes will drive improvements in ground motion prediction and seismic hazard assessment for hypothetical megathrust earthquakes expected along the Nankai Trough. However, moderate-to-large earthquakes of this focal type have become very rare in the source region in the last half century. Therefore, this event provides a unique opportunity to investigate the source characteristics related to strong motion generation of subduction-zone plate-boundary earthquakes along the Nankai Trough, southwest Japan.

In this study, the source model of the 2016 earthquake offshore the Kii peninsula was estimated through broadband strong motion waveform modeling using the empirical Green's function method to investigate the source characteristics related to strong ground motion generation during this event. The abovementioned previous works on subduction-zone plate-boundary earthquakes in Japan were implemented for events occurring along the Japan Trench in northeast Japan. We compared the source characteristics of this event with those from subduction-zone plate-boundary earthquakes in northeast Japan to illuminate and discuss the regional difference in source characteristics in terms of strong motion generation from plate-boundary earthquakes.

Source Modeling by Broadband Strong Ground Motion Simulation using the Empirical Green's Function Method

The source model of the 2016 earthquake offshore the Kii peninsula was estimated by the broadband strong motion waveform modeling using the empirical Green's function method based on the SMGA source model (Irikura, 1986; Miyake *et al.*, 2003). Detailed introduction of the concept of SMGA and the strong ground motion simulation technique using the empirical Green's function method of Irikura (1986) can be found in Miyake *et al.* (2003).

We collected near-source strong motion data recorded by accelerometers at cabled sea-floor stations of DONET1. We also collected acceleration records from the Long-Term Borehole Monitoring System (LTBMS) installed within the accretionary prism underlying the Kumano sedimentary basin at a depth of 904 m below the sea floor at station KMDB1, which was installed by JAMSTEC. Some offshore stations close to the epicenter with high peak ground accelerations were excluded in this analysis to avoid any effect of soil nonlinearity during strong shaking. In addition to offshore stations, we collected strong motion data from velocity-type strong motion sensors (Tokyo-Sokushin VSE-355G3) at onshore broadband stations in the Kii peninsula belonging to F-net of NIED (station KIS) and Disaster Prevention Research Institute (DPRI) of Kyoto University (station SMK).

The hypocenter locations of the mainshock and aftershocks were based on the hypocenter catalog of Wallace *et al.* (2016) (Figure 1). They located the mainshock and aftershocks within 48 h after the mainshock using DONET accelerometer data. The hypocenter of the mainshock in their catalog is 33.34999°N, 136.4010°E, and at a depth of 11.371 km. In addition to the M_{JMA} 6.5 mainshock, some $M3$ class aftershocks occurred on the same day. Because of their good quality, the records of an M_{JMA} 3.2 aftershock at 13:04 on 1 April 2016 (33.41679°N, 136.3475°E, at a depth of 14.186 km according to Wallace *et al.*, 2016) were selected to serve as the empirical Green's functions. The CMT solution of this aftershock is not available.

Firstly, the observed source spectral ratio between the mainshock and the aftershock, which was used as an empirical Green's function, was analyzed to objectively determine two scaling parameters N (integer) and C (real number). N gives the ratio of source dimensions between the target and EGF events. C corresponds to the ratio of stress drop between the target and EGF events. If we assume that the source spectrum follows the ω^{-2} source model (Brune, 1970, 1971), these scaling parameters obey the following relationships (e.g., Miyake *et al.*, 2003),

$$\frac{U_0}{u_0} = \frac{M_0}{m_0} = CN^3, \qquad (1)$$

$$\frac{A_0}{a_0} = \frac{M_0}{m_0} \cdot \left(\frac{f_{\mathrm{cm}}}{f_{\mathrm{ca}}}\right)^2 = CN\ . \qquad (2)$$

U_0 and u_0 are the flat levels of displacement amplitude spectra for the target and EGF events, respectively. M_0/m_0 corresponds to the seismic moment ratio between the target and EGF events. A_0 and a_0 indicate the flat levels of the acceleration amplitude spectra for the target and EGF events. f_{cm} and f_{ca} are corner frequencies of the target and the EGF events, respectively.

The scaling parameters N and C were determined using strong motion data recorded at five DONET stations, one LTBMS ocean-bottom borehole station, and two onshore strong motion stations (Figure 1). The Fourier spectrum of the S-wave part was calculated for each station from a 40.96 s window of the three-component record beginning 1 s before the S-wave arrival. A Parzen window with a bandwidth of ±5% of each frequency point was applied to the original amplitude spectra in order to smooth the amplitude spectra. The propagation path effect was corrected by geometrical spreading for the S-wave and by a frequency-dependent attenuation factor for the S-wave, $Q(f) = 182f^{0.68}$ (Shiba and Sato, 2007). The average S-wave velocity in and around the source region was assumed to be 3.45 km/s (Iwata *et al.*, 2008). The log average of the spectral ratios for all stations was employed as the observed source spectral ratio. The theoretical source spectral ratio function (SSRF) based on the ω^{-2} source model was fitted to the observed source spectral ratio by the source spectral ratio fitting method (Miyake *et al.*, 1999, 2003). SSRF was defined as

$$\mathrm{SSRF}(f) = \frac{M_0}{m_0} \frac{1+(f/f_{\mathrm{ca}})^2}{1+(f/f_{\mathrm{cm}})^2}. \qquad (3)$$

This method estimates the seismic moment ratio (M_0/m_0) and corner frequencies for the mainshock (f_{cm}) and the EGF event (f_{ca}). The observed source spectral ratio is compared with the best-fit theoretical source spectral ratio in Figure 2(a). The estimated seismic moment ratio was 2220, and the estimated corner frequencies for the mainshock and aftershock were 0.45 Hz and 3.4 Hz, respectively. From the seismic moment ratio and corner frequencies, the scaling parameters N and C were determined to be 8 and 5.1, respectively.

Finally, following the technique of Asano and Iwata (2012), we used a grid search approach and broadband ground motion simulations from the mainshock at the relevant stations to estimate the model parameters of the SMGA. In their technique the waveform $U(t)$ for the target event is computed using records of the small event $u(t)$, considered as empirical Green's functions:

$$U(t)=\sum_{i=1}^{N}\sum_{j=1}^{N}\frac{R}{R_{ij}}\left\{F(t)*\left(C\cdot u(t)\right)\right\} \quad , \tag{4}$$

$$F(t)=\delta(t-t_{ij})+\frac{1}{n'(1-e^{-1})}\cdot\sum_{k=1}^{(N-1)n'}\left[e^{-\frac{k-1}{(N-1)n'}}\cdot\delta\left(t-t_{ij}-\frac{(k-1)\tau}{(N-1)n'}\right)\right] \quad , \tag{5}$$

$$t_{ij}=T_{ij}-T_0+\frac{\xi_{ij}}{V_{\mathrm{r}}} \quad . \tag{6}$$

Here, $F(t)$ is a filter function which corrects for the difference of slip-velocity functions between the target and EGF events (Irikura, 1986; Irikura *et al.*, 1997). R is the distance along the ray path of the S-wave for the EGF event, and R_{ij} is the distance along the ray path of the S-wave from the subfault (i, j) to the station. τ is the rise time of the SMGA, and T_{ij} and T_0 represent the travel times of the S-wave from the subfault (i, j) and the hypocenter, respectively. The velocity structure models used for calculating the ray path and travel time of the S-wave are one-dimensional velocity structure models derived from the crustal velocity structure model of Iwata *et al.* (2008). ξ_{ij} is the distance from the hypocenter to the subfault

(i, j) in the SMGA, and V_r is the rupture propagation velocity inside the SMGA.

The observed acceleration time histories were band-pass filtered between 0.4 Hz and 10 Hz with a Chebyshev-type recursive filter. The selection of the lower corner frequency of the bandpass filter was dictated by the relatively low signal-to-noise ratio of EGF records below 0.4 Hz. The strike and dip angles of the SMGA are 230° and 18°, respectively, following the Global CMT solution. As no clear initial phase existed in the initial part of the observed P-wave, we fixed the absolute location (latitude, longitude and depth) of the rupture starting point of the SMGA at the hypocenter located by Wallace *et al.* (2016). The model parameters of the SMGA estimated by the grid search were length L, rise time τ, rupture starting subfault (NSL, NSW) within the SMGA, and rupture propagation velocity V_r. The width W was assumed to be equal to L. The search range and its step size for each model parameter are summarized in Table 1. The time window used in estimating the waveforms goodness-of-fit starts 1 s before the S-wave arrival, and its length was fixed at 8 s for all stations, based on residuals of the acceleration envelopes and displacement waveforms (Miyake *et al.*, 1999, 2003).

Results

The best set of source parameters estimated by the grid search (Figure 2b) is summarized in Table 1. A schematic image of the obtained source model is shown in Figure 2(c). The size of SMGA was estimated to be 4.5 km × 4.5 km = 20.3 km^2. The rupture of the SMGA primarily propagated northward or towards the down-dip direction. The rupture propagation in down-dip direction is typical of subduction-zone plate-boundary earthquakes in Japan (e.g. Kamae and Kawabe, 2004; Koketsu *et al.*, 2004; Suzuki and Iwata, 2007; Wu *et al.*, 2008). The seismic moment of the mainshock estimated by the Global CMT project is 9.18×10^{17} Nm (M_W 5.9). Thus, assuming that most of the seismic moment was released from the SMGA, the stress drop of the SMGA was estimated to be 25 MPa based on the circular crack model (Eshelby, 1957; Brune 1970, 1971). If the actual seismic moment of the SMGA is smaller than the total seismic moment, then the stress drop in the SMGA would be lower than the above estimation of 25 MPa. The seismic moment of the EGF event (m_0) was estimated to be 3.16×10^{14} Nm from the flat level of the displacement spectra at the onshore rock sites (KIS and SMK). Using the estimated seismic moment of the EGF event, the seismic moment released from the SMGA could be estimated to be $M_0^{\mathrm{SMGA}} = C \cdot N^3 \cdot m_0 = 8.25 \times 10^{17}$ (Nm). Thus, the stress drop in the

SMGA would be 22.1 MPa, which is slightly smaller than the above estimation of 25 MPa.

The comparison between the observed and the simulated acceleration, velocity, and displacement waveforms in the frequency range between 0.4 and 10 Hz at the target stations are shown in Figure 3, and Fourier spectra for those waveforms are plotted in Figure 4. The synthetic waveforms adequately explain the observed waveforms in a broad frequency range. In order to check the validity of the obtained source model, synthetic ground motions were also computed for six stations that were not used in the grid-search source modeling. These stations are indicated by * in Figure 3. Because stations KME17, KME19, and KME20 are relatively close to the epicenter, and located on soft sediments within the oceanic basin, the observed waveforms at these stations might be affected by soil nonlinear response, which was not included in our simulations. This could explain the difference between recorded and simulated waveforms at these stations.

Figure 2(b) shows the distribution of the residual in the model parameters space in which the grid search was conducted. The grid search was performed on a total of 1,915,200 models obtained by changing five rupture model parameters. The star in this figure represents the best model summarized in Table 1. The residual distribution is smooth and has only one global minimum. In particular, the direction of rupture propagation was well constrained by the data because of the good azimuthal coverage with the offshore and onshore stations.

Discussions

Asano *et al.* (2014) investigated the relationship between the seismic moment and the size of the SMGA for past subduction-zone plate-boundary earthquakes along the Japan Trench in northeast Japan (Figure 3.9d in their paper). They compiled a database of SMGA parameters in northeast Japan from previous results (e.g., Kamae and Kawabe, 2004; Miyahara and Sasatani, 2004; Suzuki and Iwata, 2005, 2007; Takiguchi et al., 2011; Asano and Iwata, 2012). The resulting SMGA for the M_W 5.9 event in the Nankai Trough is plotted with past subduction-zone plate-boundary earthquakes in northeast Japan in Figure 5. Inland crustal earthquakes in Japan analyzed and compiled by Miyake *et al.* (2003) and Miyakoshi *et al.* (2015) are also plotted in the same figure for comparing source characteristics among subduction-zone plate-boundary earthquakes and inland crustal earthquakes. As reported by Miyake *et al.* (2003), the size of the SMGA obtained by broadband strong motion simulations for inland crustal earthquakes (gray circles in Figure 5) are consistent with the empirical source scaling relationship for the combined area of asperities proposed by Somerville *et al.* (1999). However, SMGAs for subduction-zone plate-boundary earthquakes along the Japan Trench in northeast Japan (black circles in Figure 5) are systematically smaller than those for Japanese inland crustal earthquakes (Asano *et al.*, 2014). In addition, SMGAs for subduction-zone plate-boundary earthquakes in northeast Japan are smaller than those indicated by the empirical scaling relationship between the combined area of asperities and seismic moment for subduction-zone plate-boundary earthquakes by Murotani *et al.* (2008). The SMGA is smaller than asperity or large slip area for subduction-zone plate-boundary earthquakes in northeast Japan, which is a significant source characteristic differentiating subduction-zone plate-boundary earthquakes in northeast Japan from inland crustal earthquakes in Japan. Previous studies suggested that the stress drop of the SMGA for subduction-zone plate-boundary earthquakes along the Japan Trench is larger than that of inland crustal earthquakes in Japan. Such source characteristics would cause strong short-period seismic wave radiations from particular areas of the source fault.

The size of the SMGA of the M_W 5.9 earthquake in the Nankai Trough is almost similar to those for past inland crustal earthquakes in Japan with similar magnitude. Thus, our broadband ground motion modeling of this earthquake revealed different source characteristics from those of previous subduction-zone plate-boundary earthquakes along the Japan Trench in terms of generation of strong motions. This can be explained by the difference in the average characteristics of stress drop for the SMGA between the Nankai Trough and Japan Trench. Another possible reason is the depth dependency of the source rupture behavior (e.g., Bilek and Lay, 1998; Lay *et al.*, 2012) because the focal depth of this event (11 km) was within the depth range of inland crustal earthquakes, being much shallower than that of past subduction-zone plate-boundary earthquakes along the Japan Trench. Notably, this study investigated only one M_W 5.9 earthquake and a single case in the Nankai Trough. Therefore, it is likely that the results of this study are not representative of the general characteristics of the target area. Nevertheless, this work contributes to future improvements of ground motion prediction by also taking into consideration change in rupture characteristics between different subduction-zone regions in Japan. Future analysis using such ocean-bottom ground motion data would be necessary to obtain more universally applicable source characteristics for this area.

Conclusions

The SMGA source model of the 2016 M_W 5.9 (M_{JMA} 6.5) thrust-type earthquake in the Nankai Trough, offshore the Kii peninsula, southwest Japan was estimated on the basis of broadband strong ground motion waveform modeling using the empirical Green's function method. The model parameters for the SMGA were constrained by modeling broadband ground motion waveforms in the frequency range from 0.4 Hz to 10 Hz observed at offshore and onshore strong motion stations. The best estimate of SMGA size was 20.3 km^2, and its stress drop was approximately 22 MPa, which differs from that of past plate-boundary earthquakes with similar magnitude along the Japan trench, northeast Japan. This implies the possibility that the average source characteristics of plate-boundary events in the Nankai Trough are different from those along the Japan Trench. Although the results of this study were obtained for only a single case in the Nankai trough, they may provide important information for consideration of regional variations in source rupture characteristics. This will contribute to improvements of ground motion prediction for seismic hazard assessment of future megathrust earthquakes in Japan. Future studies on this topic using offshore and onshore ground motion data would be helpful to obtain more universal characteristics of source rupture behavior in this subduction zone.

Data and Resources

The strong motion data used in this study were collected from the Dense Oceanfloor Network system for Earthquake and Tsunamis (DONET) jointly operated by the National Research Institute for Earth Science and Disaster Resilience (NIED) and Japan Agency for Marine-Earth Science and Technology (JAMSTEC), the Long-Term Borehole Monitoring System of JAMSTEC, the Full Range Seismograph Network (F-net) of NIED, and Disaster Prevention Research Institute (DPRI), Kyoto University. Data of DONET and F-net are available from the NIED Hi-net website at www.whinet.bosai.go.jp (last accessed on 14 January 2017). Data of LTBMS can be obtained from the JAMSTEC Ocean-bottom Seismology Database at join-web.jamstec.go.jp/join-portal/ (last accessed on 6 June 2016). The source models of the 1944 Tonankai earthquake were retrieved from SRCMOD website (Mai and Thingbaijam, 2014) at equake-rc.info/SRCMOD/ (last accessed on 10 May 2017). The Global Centroid Moment Tensor Project database was searched using www.globalcmt.org/CMTsearch.html (last accessed on 28 November 2017). The data source of topography and bathymetry data is JTOPO30v2, which is available from the Japan Hydrographic Association. All figures were made using the Generic Mapping Tools version 5.4.1 (www.soest.hawaii.edu/gmt; Wessel *et al.*, 2013).

Acknowledgements

This study is supported by the Research Project for Compound Disaster Mitigation on the Great Earthquakes and Tsunamis around the Nankai Trough Region of the Ministry for Education, Culture, Sport, Science and Technology (MEXT), Japan; Earthquake and Volcano Hazards Observation and Research Program of MEXT; the Grant-in-Aid for Young Scientists (B) No.25750146 (PI K. Asano); and Grant-in-Aid for Scientific Research (B) No.26282104 (PI T. Iwata). The author appreciated their careful reviews by two anonymous reviewers and the associate editor Adrien Oth.

References

Ando, M. (1975). Source mechanism and tectonic significance of historical earthquakes along the Nankai trough, Japan, *Tectonophysics* **27**, 119–140, doi:10.1016/0040-1951(75)90102-X.

Asano, K., and T. Iwata (2012). Source model for strong ground motion in 0.1–10

Hz during the 2011 Tohoku earthquake, *Earth Planets Space* **64**, 1111–1123, doi:10.5047/eps.2012.05.003.

Asano, K., T. Iwata, and K. Irikura (2003). Source characteristics of shallow intraslab earthquakes derived from strong-motion simulations, *Earth Planets Space* **55**, e5–e8, doi:10.1186/BF03351744.

Asano, K., H. Sekiguchi, T. Iwata, W. Suzuki, S. Aoi, and T. Kunugi (2014), Source process of the 2011 off the Pacific coast of Tohoku earthquake, in *Studies on the 2011 Off the Pacific Coast of Tohoku Earthquake* Hiroshi Kawase (Editor), Springer Japan, Tokyo, 17–36, doi:10.1007/978-4-431-54418-0_3.

Bilek, S. L., and T. Lay (1998). Variation of interplate fault zone properties with depth in the Japan subduction zone, *Science* **281**, 1175–1178, doi:10.1126/science.281.5380.1175.

Brune, J. N. (1970). Tectonic stress and the spectra of seismic shear waves from earthquakes, *J. Geophys. Res.* **75** 4997–5009, 1970, doi:10.1029/JB075i026p04997.

Brune, J. N. (1971). Correction, *J. Geophys. Res.* **76**, 5002, 1971, doi:10.1029/JB076i020p05002.

Ekström, G., M. Nettles, and A. M. Dziewonski (2012). The global CMT project

2004-2010: Centroid-moment tensors for 13,017 earthquakes, *Phys. Earth Planet. Inter.* **200–201**, 1–9, doi:10.1016/j.pepi.2012.04.002.

Eshelby, J. D. (1957). The determination of the elastic field of an elliptical inclusion, and related problems, *Proc. Roy. Soc.* **A241**, 376–396, doi:10.1098/rspa.1957.0133.

Hashimoto, M. and D. D. Jackson (1993). Plate tectonics and crustal deformation around the Japanese Islands, *J. Geophys. Res.* **98**, 16149–16166, doi:10.1029/93JB00444

Ichinose, G. A., H. K. Thio, P. G. Somerville, T. Sato, and T. Ishii (2003). Rupture process of the 1944 Tonankai earthquake (M_S 8.1) from the inversion of teleseismic and regional seismograms, *J. Geophys. Res.* **108**, B10, 2497, doi:10.1029/2003JB002393.

Irikura, K. (1986). Prediction of strong acceleration motions using empirical Green’s function, *Proc. 7th Japan Earthq. Eng. Symp.*, Tokyo, Japan, 151–156.

Irikura, K., T. Kagawa, and H. Sekiguchi (1997). Revision of the empirical Green’s function method by Irikura (1986), *Prog. Abst. Seism. Soc. Japan*, **2**, B25 (in Japanese).

Iwata, T., T. Kagawa, A. Petukhin, and Y. Onishi (2008). Basin and crustal velocity structure models for the simulation of strong ground motions in the Kinki area, Japan, *J. Seism.* **12**, 223-234, doi:10.1007/s10950-007-9086-7.

Kamae, K., and K. Irikura (1998). Source model of the 1995 Hyogo-ken Nanbu earthquake and simulation of near-source ground motion, *Bull. Seism. Soc. Am.* **88**, 400–412:

Kamae, K., and H. Kawabe (2004). Source model composed of asperities for the 2003 Tokachi-oki, Japan, earthquake (M_{JMA} = 8.0) estimated by the empirical Green's function method, *Earth Planets Space* **56**, 323–327, doi:10.1186/BF03353059.

Kaneda Y., K. Kawaguchi, E. Araki, H. Matsumoto, T. Nakamura, S. Kamiya, K. Ariyoshi, T. Hori, T. Baba, and N. Takahashi (2015). Development and application of an advanced ocean floor network system for megathrust earthquakes and tsunamis, in *Seafloor Observatories: A New Vision of the Earth from Abyss* Paolo Favali, Laura Beranzoli, and Angelo De Santis (Editors), Springer-Verlag, Berlin Heidelberg, 643–662, doi:10.1007/978-3-642-11374-1_25.

Kawabe, H., and K. Kamae (2013). Source modeling of the 2011 off the Pacific coast of Tohoku earthquake, *J. Jpn Assoc. Earthq. Eng.* **13**(2), 75–87, doi:10.5610/jaee.13.2_75 (in Japanese with English abstract).

Kikuchi, M., M. Nakamura, and K. Yoshikawa (2003). Source rupture process of the 1944 Tonankai earthquake and the 1945 Mikawa earthquake derived from low-gain seismograms, *Earth Planets Space* **55**, 159–172, doi:10.1186/BF03351745.

Koketsu, K., K. Hikima, and S. Miyazaki (2004). Joint inversion of strong motion and geodetic data for the source process of the 2003 Tokachi-oki, Hokkaido, earthquake, *Earth Planets Space* **56**, 329−334, doi:10.1186/BF03353060.

Kurahashi, S., K. Masaki, and K. Irikura (2008). Source model of the 2007 Noto-Hanto earthquake (M_W 6.7) for estimating broad-band strong ground motion, *Earth Planets Space* **60**, 89–94, doi:10.1186/BF03352766.

Kurahashi, S., and K. Irikura (2010). Characterized source model for simulating strong ground motions during the 2008 Wenchuan earthquake, *Bull. Seism. Soc. Am.* **100**, 2450–2475, doi:10.1785/0120090308.

Kurahashi, S., and K. Irikura (2013). Short-period source model of the 2011 Mw 9.0 off the Pacific coast of Tohoku earthquake, *Bull. Seism. Soc. Am.* **103**, 1317–1393, doi:10.1785/0120120157.

Lay, T., H. Kanamori, C. J. Ammon, K. D. Koper, A. R. Hutko, L. Ye, H. Yue, and

T. M. Rushing (2012). Depth-varying rupture properties of subduction zone megathrust faults, *J. Geophys. Res.* **117**, B04311, doi:10.1029/2011JB009133.

Maeda, T., M. Ichiyanagi, H. Takahashi, R. Honda, T. Yamaguchi, M. Kasahara, and T. Sasatani (2008). Source parameters of the 2007 Noto Hanto earthquake sequence derived from strong motion records at temporary and permanent stations, *Earth Planets Space* **60**, 1011–1016, doi:10.1186/BF03352861.

Maeda, T., and T. Sasatani (2009). Strong ground motions from an M_j 6.1 inland crustal earthquake in Hokkaido, Japan: the 2004 Rumoi earthquake, *Earth Planets Space* **61**, 689–701, doi:10.1186/BF03353177.

Maeda, T., A. Iwaki, N. Morikawa, S. Aoi, and H. Fujiwara (2016). Seismic-hazard analysis of long-period ground motion of megathrust earthquakes in the Nankai trough based on 3D finite-difference simulation, *Seism. Res. Lett.* **87**, 1265–1273, doi:10.1785/0220160093.

Mai, P. M., and K. K. S. Thingbaijam (2014). SRCMOD: An online database of finite-fault rupture models, *Seism. Res. Lett.* **85**, 1348–1357, doi:10.1785/0220140077.

Miyahara, S., and T. Sasatani (2004). Estimation of source process of the 1994 Sanriku Haruka-oki earthquake using empirical Green's function method, *Geophys. Bull. Hokkaido Univ.* **67**, 197–212. (in Japanese with English abstract)

Miyake, H., T. Iwata, and K. Irikura (1999). Strong ground motion simulation and source modeling of the Kagoshima-ken Hokuseibu earthquakes of March 26 (M_{JMA} 6.5) and May 13 (M_{JMA} 6.3), 1997, using empirical Green's function method, *Zisin 2* (*J. Seism. Soc. Jpn.*) **51**, 431–442, doi:10.4294/zisin1948.51.4_431. (in Japanese with English abstract)

Miyake, H., T. Iwata, and K. Irikura (2003). Source characterization for broadband ground-motion simulation: Kinematic heterogeneous source model and strong motion generation area, *Bull. Seism. Soc. Am.* **93**, 2531–2545, doi:10.1785/0120020183.

Miyake, H., K. Koketsu, and T. Furumura (2008). Source modeling of subduction-zone earthquakes and long-period ground motion validation in the Tokyo metropolitan area, *Proc. Fourteenth World Conf. Earthq. Eng.*, Beijing, China, paper no. S10-012.

Miyakoshi, K., K. Irikura, and K. Kamae (2015). Re-examination of scaling relationships of source parameters of the inland crustal earthquakes in Japan based on the waveform inversion of strong motion data, *J. Jpn. Assoc. Earthq. Eng.* **15**(7), 141–156, doi:10.5610/jaee.15.7_141. (in Japanese with English abstract)

Murotani, S., H. Miyake, and K. Koketsu (2008). Scaling of characterized slip models for plate-boundary earthquakes, *Earth Planets Space* **60**, 987–991, doi:10.1186/BF03352855.

Oth, A., F. Wenzel, and M. Radulian (2007). Source parameters of intermediate-depth Vrancea (Romania) earthquakes from empirical Green's functions modeling, *Tectonophysics* **438**, 33–56, doi:10.1016/j.tecto.2007.02.016.

Poiata, N., and H. Miyake (2017). Broadband ground motion simulation of the 2004 and 1977 Vrancea, Romania, earthquakes using the empirical Green’s function method, *Pure Appl. Geophys.* **174**, 3503–3519, doi:10.1007/s00024-017-1605-z.

Poiata, N., K. Koketsu, A. Vuan, and H. Miyake (2012). Low-frequency and broad-band source models of the 2009 L’Aquila, Italy, earthquake, *Geophys. J. Int.* **191**, 224–242, doi:10.1111/j.1365-246X.2012.05602.x.

Ramírez-Gaytán, A., J. Aguirre, C. I. Huerta-López, and R. Vazquez-Rosas (2010). Simulation of accelerograms, peak ground accelerations, and MMI for the Tecomán earthquake of 21 January 2003, *Bull. Seism. Soc. Am.* **100**, 2163–2173, doi:10.1785/0120090053.

Riahi, A., H. Sadeghi, and S. K. Hosseini (2015). Simulation of 2003 Bam (Iran) earthquake using empirical Green's function method via very small and near-fault events, *Geophys. J. Int.* **201**, 1264–1286, doi:10.1093/gji/ggv074.

Satoh, T. (2012). Source modeling of the 2011 off the Pacific coast of Tohoku earthquake using empirical Green's function method –From the viewpoint of the short period spectral level of interplate earthquakes–, *J. Struct. Constr. Eng., AIJ* **77**, 695–704, doi:10.3130/aijs.77.695. (in Japanese with English abstract)

Sekiguchi, H., M. Yoshimi, H. Horikawa, K. Yoshida, S. Kunimatsu, and K. Satake (2008). Prediction of ground motion in the Osaka sedimentary basin associated with the hypothetical Nankai earthquake, *J. Seism.* **12**, 185–195, doi:10.1007/s10950-007-9077-8.

Seno, T., S. Stein, and A. E. Gripp (1993). A model for the motion of the Philippine Sea Plate consistent with NUVEL-1 and geological data, *J. Geophys. Res.* **98**, 17941–17948, doi:10.1029/93JB00782.

Shiba, Y., and H. Sato (2007). Source and path characteristics of earthquakes occurring off the Kii peninsula, *CRIEPI Research Report*, N07007, 22pp.

Suzuki, W. and T. Iwata (2005). Source characteristics of interplate earthquakes in northeast Japan inferred from the analysis of broadband strong-motion records, *Eos Trans. Am. Geophys. Union* **86**(52), Fall Meet. Suppl., Abstract S43A-1040.

Suzuki, W. and T. Iwata (2006). Source model of the 2005 west off Fukuoka prefecture earthquake estimated from the empirical Green's function simulation of broadband strong motions, *Earth Planets Space* **58**, 99–104, doi:10.1186/BF03351921.

Suzuki, W., and T. Iwata (2007). Source model of the 2005 Miyagi-oki, Japan, earthquake estimated from broadband strong motions, *Earth Planets Space* **59**, 1155–1171, doi:10.1186/BF03352063.

Takiguchi, M., K. Asano, and T. Iwata (2011). The comparison of source models of repeating subduction zone earthquakes estimated using broadband strong motion records −1982 and 2008 Ibarakiken-oki M7 earthquakes–, *Zisin 2* (J. Seismol. Soc. Japan) **63**, 223–242, doi:10.4294/zisin.63.223. (in Japanese with English abstract)

Wallace, L. M., E. Araki, D. Saffer, X. Wang, A. Roesner, A. Kopf, A. Nakanishi, W. Power, R. Kobayashi, C. Kinoshita, S. Toczko, T. Kimura, Y. Machida, and S. Carr (2016). Near-field observations of an offshore Mw 6.0 earthquake from an integrated seafloor and subseafloor monitoring network at the Nankai

Trough, southwest Japan, *J. Geophys. Res.* **121**, 8338–8351, doi:10.1002/2016JB013417.

Wen, Y.-Y., H. Miyake, Y.-T. Yen, K. Irikura, and K.-E. Ching (2014). Rupture directivity effect and stress heterogeneity of the 2013 Nantou blind-thrust earthquakes, Taiwan, *Bull. Seism. Soc. Am.* **104**, 2933–2942, doi:10.1785/0120140109.

Wen, Y.-Y., S.-Y. Chao, Y.-T. Yen, and S. Wen (2017). Source characteristics of moderate-to-strong earthquakes in the Nantou area, Taiwan: insight from strong ground motion simulations, *Earth Planets Space* **69**:132, doi:10.1186/s40623-017-0720-5.

Wessel, P., W. H. F. Smith, R. Scharroo, J. F. Luis, and F. Wobbe (2013). Generic Mapping Tools: Improved version released, *Eos Trans. Am. Geophys. Union* **94**(45), 409–413, doi: 10.1002/2013EO450001.

Wu, C., K. Koketsu, and H. Miyake (2008). Source processes of the 1978 and 2005 Miyagi-oki, Japan earthquakes: Repeated rupture of asperities over successive large earthquakes, *J. Geophys. Res.* **113**, B08316, doi:10.1029/2007JB005189.

Xia, C., B. Zhao, M. Horike, and T. Kagawa (2015). Strong ground simulations of the M_{W} 7.9 Wenchuan earthquake using the empirical Green's function method, *Bull. Seism. Soc. Am.* **105**, 1383–1397, doi:10.1785/0120140001.

Yamamoto, Y., and H. Takenaka (2009). Source modeling of the 2007 Niigataken Chuetsu-oki earthquake using the empirical Green’s function method, *Zisin 2* (J. Seismol. Soc. Japan) **62**, 47–59, doi:10.4294/zisin.62.137. (in Japanese with English abstract)

Full mailing address of the author

Disaster Prevention Research Institute, Kyoto University, Gokasho, Uji, Kyoto 611-0011, Japan

k-asano@sms.dpri.kyoto-u.ac.jp

(K.A.)

Table 1 Search range, grid interval, and estimated value of model parameters in the grid search

	Search range	Interval	Estimated value
Length L (km)	0.8–14.0	0.1	4.5
Rise time τ (s)	0.08–1.2	0.08	0.32
Rupture starting subfault in strike direction NSL	1–8	1	6
Rupture starting subfault in dip direction NSW	1–8	1	3
Rupture velocity V_r (km/s)	2.2–3.6	0.1	3.3

List of Figure Captions

Figure 1. Map showing the studied area. The rectangle indicated by dotted lines in the left panel corresponds to the geographical area drawn in the right panel. The stars represent the epicenters of the mainshock of the 2016 offshore the Kii peninsula earthquake (open star) and the EGF event (solid star) located by Wallace *et al.* (2016). The moment tensor solution by the Global CMT Project (lower hemisphere projection) is shown inside the left panel. Brown and magenta contours represent the slip distributions of the 1944 Tonankai earthquake estimated by Kikuchi *et al.* (2003) and Ichinose *et al.* (2003), respectively. The blue, red, and black triangles indicate seafloor (DONET), ocean-bottom borehole (LTBMS), and inland broadband seismic stations, respectively.

Figure 2. (a) Observed source spectral ratios between the target and EGF events at each strong motion station (thin gray lines) and average observed source spectral ratio (thick line). The red curve represents the theoretical source spectral ratio based on the ω^{-2} source model for the best estimate. The solid and open triangles indicate the corner frequency of the target and EGF events, respectively. (b) Distribution of

residual values obtained by the grid search method. The star indicates the best estimate. (c) Schematic illustration of the obtained SMGA source model. The solid star indicates the rupture starting point.

Figure 3. Comparison between observed (gray) and synthetic (black) acceleration, velocity, and displacement waveforms in the frequency range 0.4–10 Hz. Two horizontal components are shown. The stations with asterisk were not used in source modeling by the grid search.

Figure 4. Comparison between the Fourier amplitude spectra of the observed (gray) and simulated acceleration waveforms (black).

Figure 5. Scaling relationship between the SMGA and total seismic moment. The star represents the M_W 5.9 event in the Nankai Trough analyzed in this study. The black and gray circles indicate past subduction-zone plate-boundary earthquakes and inland crustal earthquakes in Japan, respectively. The solid lines show the empirical scaling relationship of the combined area of asperity by Murotani *et al.* (2008) for subduction-zone plate-boundary earthquakes and Somerville *et al.* (1999)

for inland crustal earthquakes.

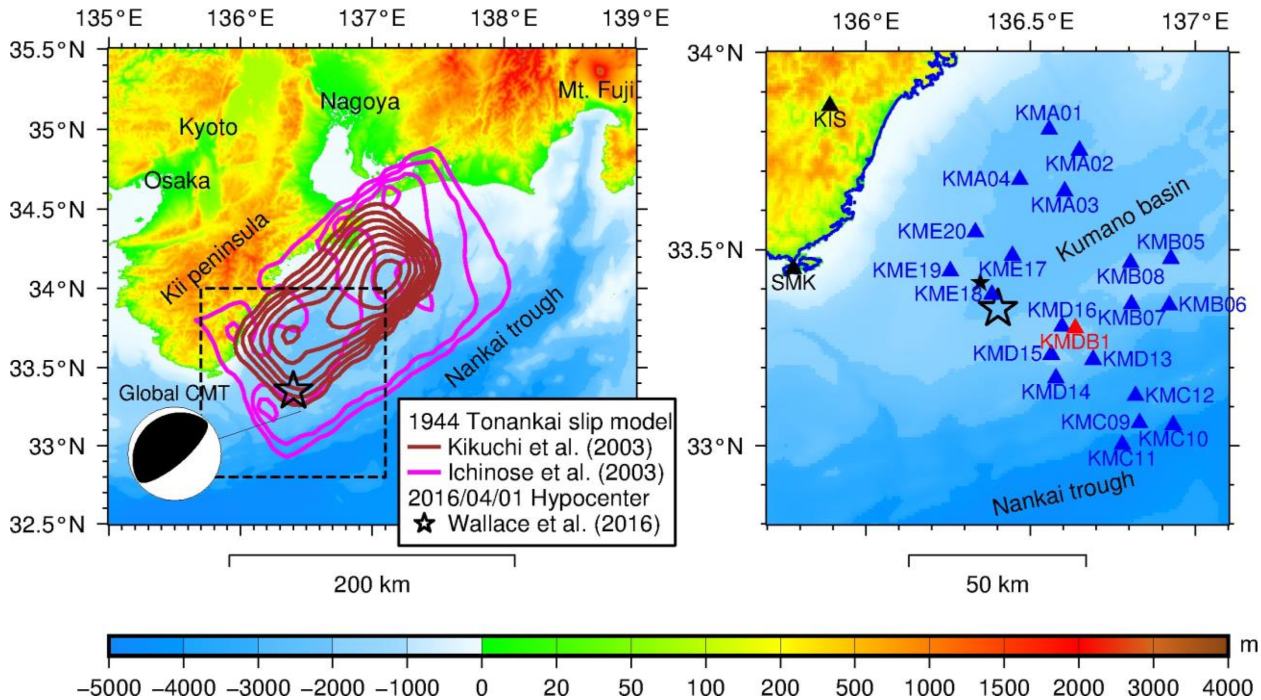

Figure 1. Map showing the studied area. The rectangle indicated by dotted lines in the left panel corresponds to the geographical area drawn in the right panel. The stars represent the epicenters of the mainshock of the 2016 offshore the Kii peninsula earthquake (open star) and the EGF event (solid star) located by Wallace *et al.* (2016). The moment tensor solution by the Global CMT Project (lower hemisphere projection) is shown inside the left panel. Brown and magenta contours represent the slip distributions of the 1944 Tonankai earthquake estimated by Kikuchi *et al.* (2003) and Ichinose *et al.* (2003), respectively. The blue, red, and black triangles indicate seafloor (DONET), ocean-bottom borehole (LTBMS), and inland broadband seismic stations, respectively.

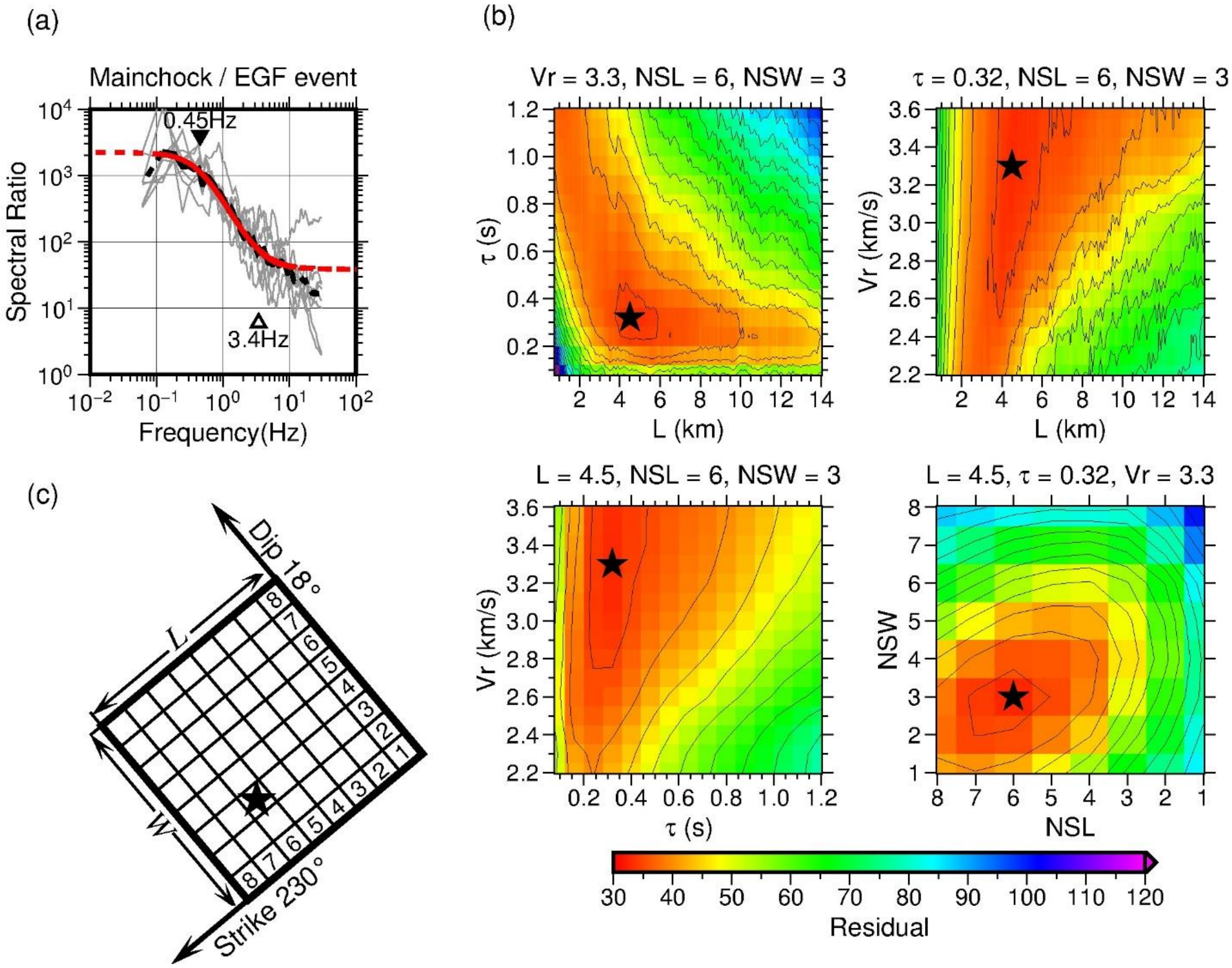

Figure 2. (a) Observed source spectral ratios between the target and EGF events at each strong motion station (thin gray lines) and average observed source spectral ratio (thick line). The red curve represents the theoretical source spectral ratio based on the ω^{-2} source model for the best estimate. The solid and open triangles indicate the corner frequency of the target and EGF events, respectively. (b) Distribution of residual values obtained by the grid search method. The star indicates the best estimate. (c) Schematic illustration of the obtained SMGA source model. The solid star indicates the rupture starting point.

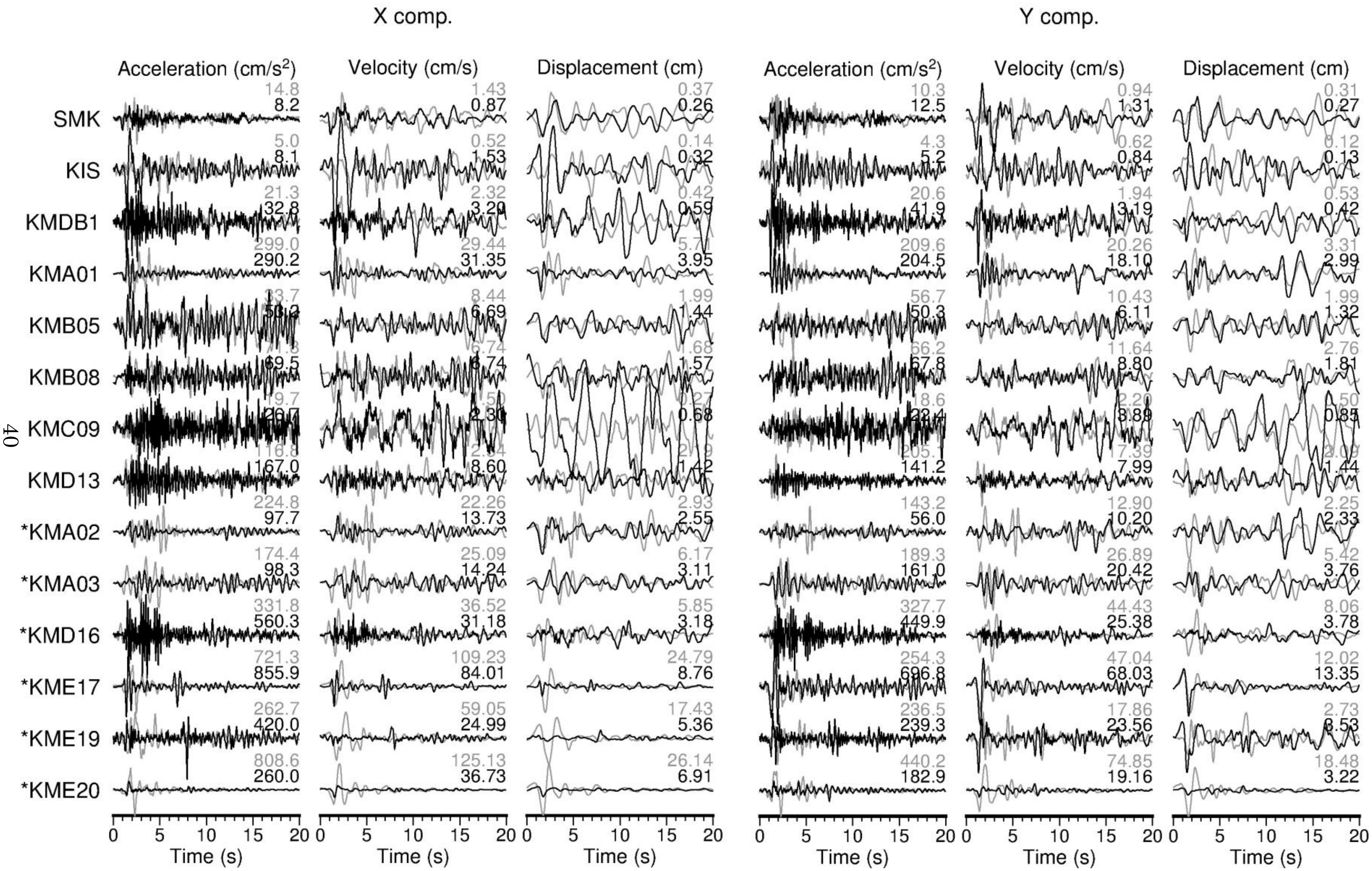
X comp.
Y comp.
Acceleration (cm/s2)
Velocity (cm/s)
Displacement (cm)
SMK
KIS
KMDB1
KMA01
KMB05
KMB08
KMC09
KMD13
*KMA02
*KMA03
*KMD16
*KME17
*KME19
*KME20
Time (s)

Figure 3. Comparison between observed (gray) and synthetic (black) acceleration, velocity, and displacement waveforms in the frequency range 0.4–10 Hz. Two horizontal components are shown. The stations with asterisk were not used in source modeling by the grid search.

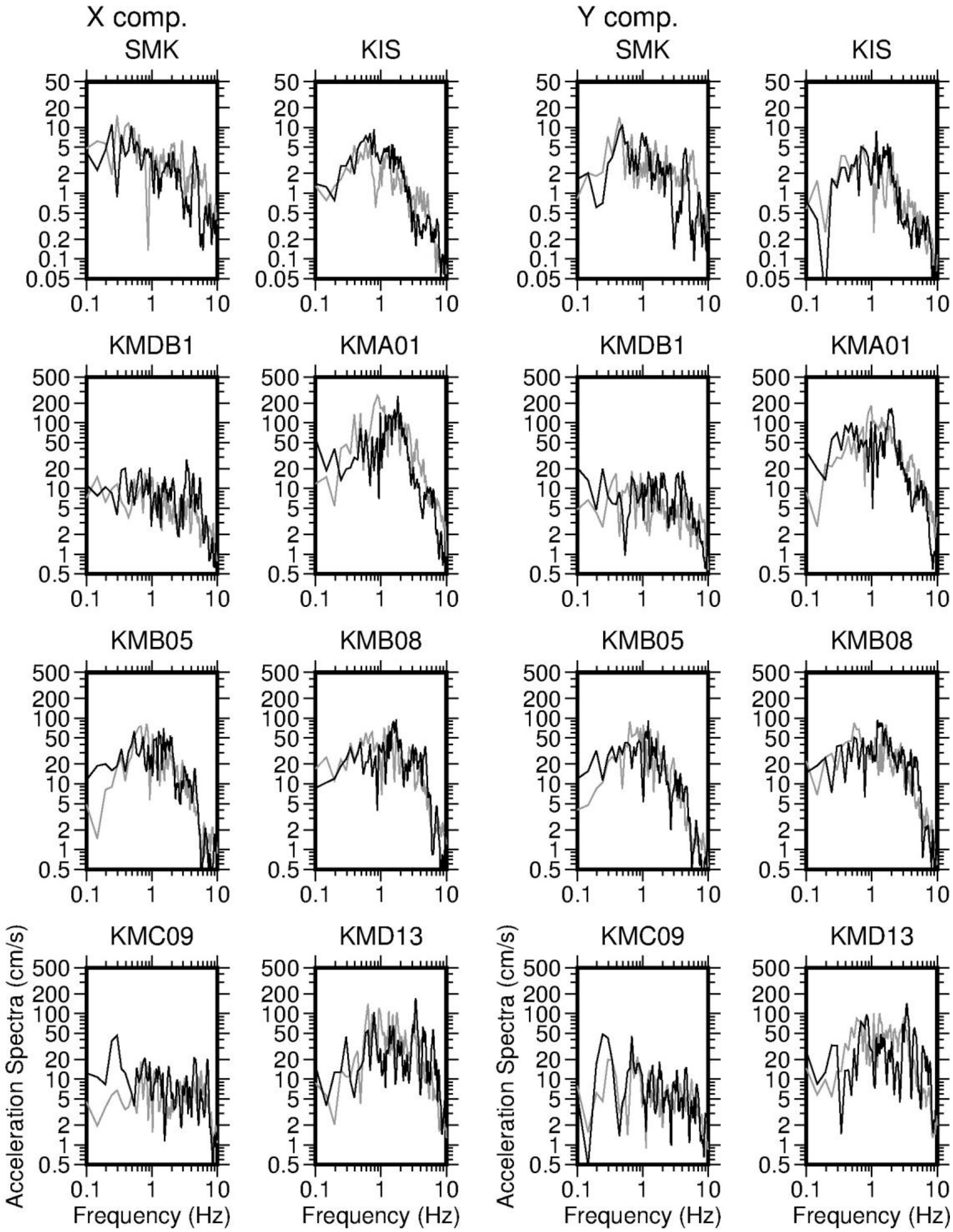

Figure 4. Comparison between the Fourier amplitude spectra of the observed (gray) and simulated accelerations (black).

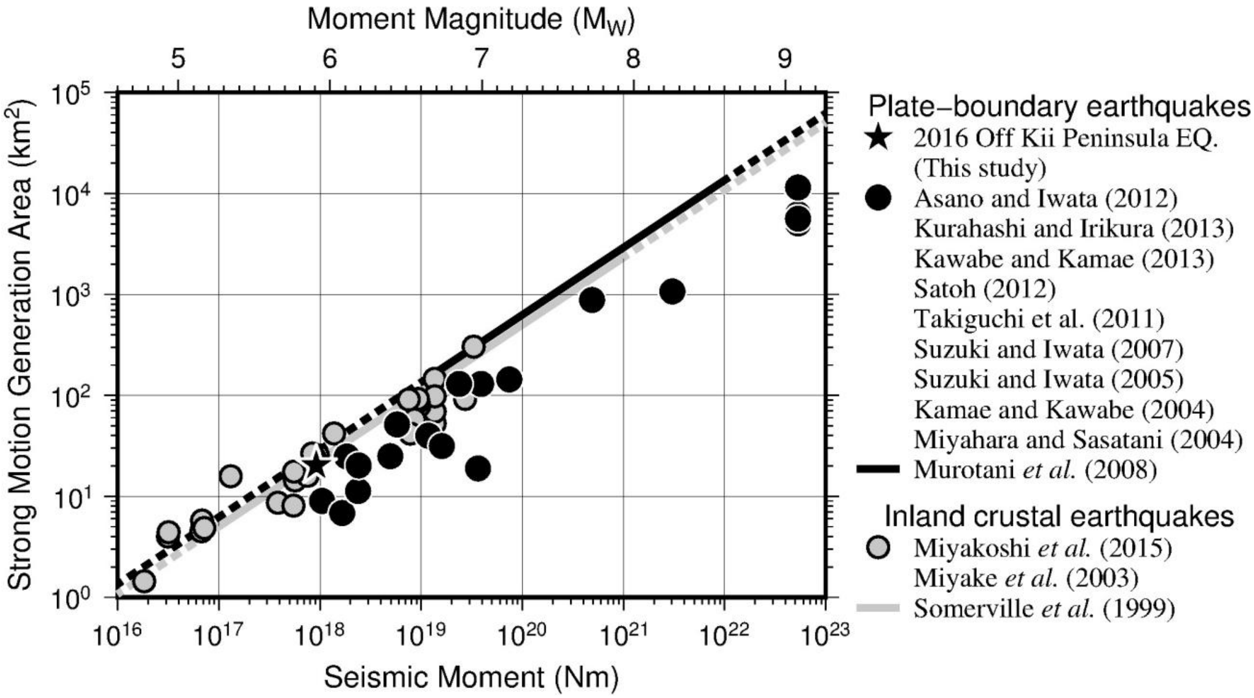

Figure 5. Scaling relationship between the SMGA and total seismic moment. The star represents the M_W 5.9 event in the Nankai Trough analyzed in this study. The black and gray circles indicate past subduction-zone plate-boundary earthquakes and inland crustal earthquakes in Japan, respectively. The solid lines show the empirical scaling relationship of the combined area of asperity by Murotani *et al.* (2008) for subduction-zone plate-boundary earthquakes and Somerville *et al.* (1999) for inland crustal earthquakes.